In-situ high temperature stress analysis of Ti(C,N) coatings on functionally graded cemented carbides by energy dispersive synchrotron X-ray diffraction

José García[1,*], Haroldo Pinto[2], Esteban Ramos-Moore[3], Carlos Espinoza[3], Jonas Östby[1], Rodrigo Coelho[4,5]

[1] AB Sandvik Coromant R&D, Lerkrogsvägen 19, SE-12680 Stockholm, Sweden.

[2] Escola de Engenharia de São Carlos, Universidade de São Paulo, CEP 13566-590, São Carlos-SP, Brazil.

[3] Facultad de Física, Pontificia Universidad Católica de Chile, Santiago 7820436, Chile.

[4] Former at Helmholtz Zentrum Berlin für Materialien und Energie GmbH, Albert Einstein St. 15, D-12489, Berlin, Germany.

[5] Now at SENAI-CIMATEC, Instituto de Inovação em Conformação e União de Materiais, Av. Orlando Gomes, 1845, Piatã, 41650-010, Salvador-BA, Brazil.

Abstract

We report on *in-situ* high temperature X-ray thermal stress analysis of chemically graded Ti(C,N) coatings deposited on functionally graded cemented carbide substrates by chemical vapor deposition. The *in-situ* analyses were performed by energy dispersive X-ray diffraction using synchrotron radiation. The samples were subjected to one individual thermal cycle from room temperature to 800°C and cooled down to room temperature again. The stresses were determined using the $\sin^2\psi$ method in the Ψ geometry combined with scattering vector measurements in order to unravel the compositional influences on the lattice strain distributions. It was found that the Ti(C,N) thin film presents a cycling residual stress

1

behavior (tensile-compressive-tensile) connected to the temperature cycle. If top-blasting is applied on the thin film layer after the coating process, compressive stresses are generated. These compressive stresses induced by top-blasting are partially released after the high temperature thermal cycle. The functionalization of the cemented carbide substrate influences the level of stresses developed in the coating. The stress behavior as a function of temperature is discussed with the support of finite element modeling by introducing a bi-linear plasticity model to calculate strain relationships which is in agreement with the synchrotron measurements.

Keywords: *In-situ* high temperature stress analysis; energy dispersive X-ray diffraction; synchrotron radiation; scattering vector; thermal stress; Ti(C,N) coatings; functionally graded cemented carbides; EBSD; finite element modeling.

*Corresponding Author: jose.garcia@sandvik.com

1. Introduction

Coated cemented carbide inserts are widely used as cutting tools for machining of metallic alloys [1]. The cemented carbide substrates are coated with wear resistant thin monolayers or multilayers (i.e. Ti(C,N), Al_2O_3, (Ti,Al)N) by chemical vapor deposition (CVD) and/or physical vapor deposition (PVD) [2]. Residual stresses in coated inserts with sharp interfaces are known to be detrimental in coating adhesion and to enhance crack propagation. The reason is that at sharp interfaces concentration of stresses develops due to the mismatches of thermal expansion coefficient (TEC) between the coating and the substrate. Surface conditioning by graded interlayers influences both coating adhesion and thermal stress evolution. It has been shown that the introduction of a graded interlayer with a continuous

transition in the material properties of a two-fold multilayer material leads to a continuous change in the stress intensity factor if cracks propagate between two layers. This is due to a redistribution of the stress field and the reduction of the pile-up of stresses if a graded interface is introduced to replace a sharp interface [3].

The production of functionally graded outer-surfaces of a few micrometers in cemented carbide substrates prior to coating deposition is of advantage for many machining applications. Surface layers enriched in binder phase and depleted of cubic carbides (known as γ-phase free layers) increase the surface toughness of the cemented carbide coating composite by reducing the propagation of thermal cracks originated in the coating during machining operations. Surface layers enriched with cubic carbides (known as γ-phase rich layers) enhance the wear-resistance of the cemented carbide coating composite [4]. Moreover it has been found that by post-treatments such as top-blasting on coatings, high compressive stresses can be induced in the coatings which enhance the performance of the coating-cemented carbide bodies [5,6].

At interrupted machining conditions, the cutting tools are subjected to load and heat cycling conditions, which influence the wear type of the tools. During interrupted cutting, the force and temperature loads have considerable higher values during material removal compared to the non-removal part of the machining step. Cracks may originate due to this thermo-mechanical cycling conditions. In particular, the mismatches of TEC between the coatings and the cemented carbide substrates during milling operations may lead to the development of stresses during the cycling conditions, which may accelerate the formation and propagation of cracks and failure of the tools [7]. In a recent work Teppernegg et al. [8] investigated by X-ray diffraction (XRD) the evolution of residual stresses in milling inserts at different steps of the tool life and correlated this information to the formation of thermo-mechanical cracks. They observed that the initial compressive stresses of the WC phase turned out in tensile

3

stresses after 1000 tool-workpiece contacts (ca. 1% of total tool life). Furthermore the level of tensile stresses was dependent on the type of wear formed in the tool, being lower when thermo-mechanical cracks appeared.

In this work we investigate *in-situ* the thermal stress behavior of Ti(C,N) deposited on graded cemented carbides during an individual thermal cycle. The thermal stresses developed in Ti(C,N) on different functionally graded surface cemented carbides are compared. The cemented carbide surfaces have a tough Co-enriched gradient zone and a wear-resistant cubic carbide rich surface [4]. Moreover, the Ti(C,N) coatings were produced by a modified CVD process, which generates a chemical gradient of carbon and nitrogen [9]. One set of samples was top-blasted in order to investigate the effect of different initial stress conditions on the coating layers. The effect of the temperature variation on the stress state of Ti(C,N) was evaluated by energy-dispersive X-ray diffraction (EDXRD) using synchrotron radiation. It is shown that the several diffraction lines measured simultaneously in each energy-dispersive diffractogram using a white incident X-ray beam allow for the evaluation of the in-plane coating stresses during a thermal cycle in the case of moderate texture formation. A combination of the $\sin^2\psi$ method [10] with independent scattering vector [11] measurements was applied to unravel the compositional influences on the lattice strain distributions. Finally, finite element modeling (FEM) was performed by considering a bi-linear plasticity in order to corroborate the EDXRD data.

2. Material and Methods

2.1. Samples

Cemented carbide substrates were produced by conventional powder metallurgy techniques, including mixing of raw powders, pressing, dewaxing and sintering at liquid phase temperatures. Functionally graded outer-layers were manufactured in the substrates by

diffusion-controlled processes during sintering according to the methods described in Ref [4]. Table 1 summarizes the composition and TEC of the substrates and functionally graded layers used in this work. The substrates were coated in a CVD-hot-wall reactor in a second step with Ti(C,N) films. A thin protective TiN layer of around 0.3 μm was first deposited at 850 °C followed by the Ti(C,N) coating deposited by a modified CVD-process in which the temperature increases at a constant rate during the process [9]. After deposition a set of coatings was subjected to blasting treatment using Al_2O_3 slurry at 1.0 bar of pressure.

Microstructure characterization was carried out by optical microscopy, scanning electron microscopy (SEM) and electron backscattering diffraction (EBSD). The SEM and EBSD analyses were conducted using a Helios NanoLab TM600 dual beam microscope (FEI Company) equipped with the EDAX/TSL EBSD system. The analyses were carried out on the sample cross section. The samples were subjected to standard metallographic grinding and polishing using OPS finishing for better visualization of the grain structure. After sample cleaning using distilled water and isopropanol, EBSD was carried out using a 20kV/22nA electron beam. The measurements were conducted in 2 steps. First the coating was scanned by considering only the TiC phase using 50 nm of step size. Then the substrate was scanned by considering the TiC and WC phases using 100 nm of step size. The grains were defined as at least two adjacent points with similar orientation within a range of 5° of misorientation. The raw data was cleaned using confidence index standardization and filtering with a cut value of 0.1. The chemical gradient of the coating layers was characterized by an electron probe micro-analysis (EPMA) Jeol JXA8530F equipped with an EDS/WDS detector using Sandvik Coromant R&D internal standards. The parameters were: beam energy of 15kW/50nA, a probe diameter of 1 mm and a dwell time of 1000 ms.

2.2. Stress Analysis

The thermal stresses in the Ti(C,N) coatings were analyzed *in-situ* using EDXRD with synchrotron radiation. The $\sin^2 \psi$ method was used to determine the stress values, whereas the scattering vector method allowed for the assessment of the unstrained lattice spacing depth profile in the chemically graded Ti(C,N) layer. The analysis of the thermal influence on the residual stress behavior for each material was conducted *in-situ* at three different stages: at room temperature before the heat treatment; at the high temperature (800°C) and at room temperature after the heat treatment. Heating was accomplished by using an Anton Paar resistance furnace, which allowed stabilization of the desired high temperature in approximately 10 min. The temperature was measured by a thermocouple fixed to the surface of the sample. A constant argon gas flowed through the furnace in order to prevent the oxidation of the coating.

In order to determine the thermal stresses in the Ti(C,N) coatings, the fundamental equation of stress analysis using XRD was applied. For a given hkl reflection, the relation between the elastic strain (ε^{hkl}_{ψ}) obtained for a certain (hkl) diffraction line at different ψ directions of the sample and $\sin^2\psi$ is presented in Eq. 1, according to the description of Noyan et al. [10]

$$\varepsilon^{hkl}_{\psi} = \frac{d^{hkl} - d^{hkl}_0}{d^{hkl}_0} = \frac{1}{2}S_2(hkl)\sigma_{//}\sin^2\psi + 2S_1(hkl)\sigma_{//} \qquad (1)$$

The term d^{hkl} is the measured spacing of a (hkl) lattice plane, d^{hkl}_0 is the strain-free lattice spacing, $S_1(hkl)$ and $\frac{1}{2}S_2(hkl)$ are the X-ray elastic constants, and $\sigma_{//}$ is the in-plane stress for the case of a stress state with rotational symmetry with respect to the normal of the sample surface. This expression can be applied to polycrystalline films without sharp preferential orientation of growth under the assumption that no shear stresses are present, the stress has in-

plane isotropy and there are none out-of-plane stress components [12].

The XRD experiments using ED synchrotron diffraction were performed at the Material Science Beamline EDDI (Energy-Dispersive Diffraction) of the Helmholtz-Zentrum Berlin at the storage ring BESSY in Berlin, Germany [13]. In EDXRD all diffraction lines are generated simultaneously by the different radiation energies of the polychromatic primary X-ray beam at a fixed 2θ-position for each diffractometer setting of the sample. The penetration depth (τ^{hkl}) does not only depend on the diffraction angle 2θ and the sample tilt ψ, but becomes also a function of the rotation angle around the diffraction vector (η), the diffraction plane (hkl), and the linear absorption coefficient μ^{hkl} that also depends on the photon energy E^{hkl}, as described in Eq. 2.

$$\tau^{hkl} = \frac{sin^2\theta - sin^2\psi + cos^2\theta \ sin^2\psi \ sin^2\eta}{2\mu(E^{hkl}) \ sin\theta sin\psi} \qquad (2)$$

According to Eq. 2 information regarding the depth distribution of the unstrained lattice spacing in the chemically graded Ti(C,N) coatings can be obtained using the scattering vector method [9], which is based on the lattice spacing depth profiling by the rotation η of the sample around the scattering vector at a strain-free coating orientation. In the x-ray stress analyses using the $sin^2\psi$ method it is assumed that the diffraction elastic constants of the coating do not change as a function of depth. A depth profile of the strain free d(hkl)-spacing was determined through scattering vector measurements. Therefore, similar results will be found if the strain free d(hkl)-spacing is assumed to be constant. The d_0^{hkl}-gradients obtained by scattering vector measurements can be least-squares fitted in order to interpolate and extrapolate the $d_0^{hkl}(\tau^{hkl})$-depth profiles, as described in our previous work [14]. This finally

enables the correction of each ε^{hkl}_{ψ}-$\sin^2\psi$ distribution with respect to the compositional lattice spacing variations within the chemically graded Ti(C,N) coatings.

2.3 FEM modeling method

The FEM program ANSYS was used to estimate the stresses from the coating process through cross-sections of coated cemented carbide substrates. The geometries of substrates were meshed as solid structures using 2-dimensional 4-node quadrilateral elements with rotational symmetry around axes perpendicular to the coating surfaces. The elements in the coatings and near-surface regions of substrates were carefully mesh-controlled to be rectangular with aspect ratios below 19. Thermo-mechanical contacts were modeled as perfectly bonded. To allow for thermal expansion, the substrate bottom plane far from the coating was constrained in displacement only along the rotational symmetry axis, and only one point in the axis was fully constrained in displacement.

All the substrate bulks were modeled as isotropic cemented carbides with a stress-free reference temperature at 22 °C. Thin film Ti(C,N)-coatings were modeled using multiple isotropic layers with thicknesses in the range 0.2 - 1 µm and with different strain-free spacings to represent the compositional gradients resulting from the modified CVD process. The layers were meshed using multiple elements up to 0.25 µm in thickness. A thin TiN layer of 0.3 µm was applied at 850 °C. Subsequent layers were applied at temperatures that were estimated from constant heating and growth rates between 900 and 1050 °C, in accordance with the experimental parameters used in the coating processes. Each coating layer composition was calculated from measured N/C ratios through the coatings, as shown in Fig. 3. The layers were applied by activating pre-meshed inactive elements at stress-free reference temperatures, and for each deposition temperature condition, a structural analysis was also performed to ensure that thermal strains in the underlying layers would be representative of

the physical coating conditions.

After deposition, thermal stresses were calculated in multiple steady-state load steps at uniform substrate temperatures.

Thermal dependences of Young's moduli (Y_M) were modeled based on published data from Refs. [15-17] and additional data on compositional dependences were included from a work by Karlsson et al. [18], resulting in the following estimation:

$$Y_M = 602 - 50x - 0.073T \text{ (GPa)} \qquad (3)$$

where x represents the carbon ratio in $TiC_xN_{(1-x)}$.

Mean thermal expansion coefficients were taken from Ref. [19] and recalculated for each layer composition and its reference temperature. The bulk material was modeled based on internal databases from Sandvik Coromant R&D with Young's moduli in similar ranges as the coating. The mean thermal expansion coefficients were in the range 4.7 to 6.6 10^{-6}/K and a constant Poisson's ratio of 0.22 was used for all the materials.

Some analyses included bi-linear isotropic plasticity in the coatings. Attention was paid to ensure that stress levels do not exceed plastic yield limits before all the elements were activated. Tensile yield limits in the range 100 to 400 MPa were considered reasonable based on the limited data available; see e.g. Ref. [20].

3. Results and Analysis

3.1. Characterization of Coating Systems

Optical and SEM images of the coating systems in the as-coated condition are shown in Fig. 1. All samples show the thin protective TiN layer of around 0.3 µm as a yellowish interface between the coatings and the substrates. The cemented carbide substrates with tough-graded

layer (γ-phase free) and with wear-resistant layer (γ-phase rich) present a different microstructure than the WC-Co hardmetal substrate; not only in the region close to the interface, but also in the bulk zone due to differences in elemental compositions, as presented in Table 1. The elemental compositions of the substrate graded layers were measured by SEM-EDS as described in Refs. [21,22].

The EBSD inverse pole figure maps of the coating systems are shown in Fig. 2. The maps pictures are montages of the coating and substrates scans in order to improve the visualization and brightness. These maps also include the image quality figure map and therefore all the points were the pattern was diffused appear in black, e.g. interfaces. Indeed, the gradient zones below the cemented carbide coatings show a significant discontinuity at the γ-phase free (Fig. 2B) and γ-phase rich (Fig. 2C) zones. This can be correlated with differences in sample preparation, chemical composition and/or grain sizes between coatings and substrates. Indeed, during metallographic preparation, the coating/substrate interfaces show a height step due to the grinding and polishing processes. Moreover, pattern distortions can be caused by chemical gradients that lead to fine grain sizes below 100 nm, which was defined as the minimum grain size. As observed in Fig. 2C, the maps of the Ti(C,N) phase deposited onto substrates A and C systems show a weak preferred <110> texture with a maximum of 2.3 texture index, in correlation with coatings fabricated by modified-CVD [23,24]. The Ti(C,N) coating deposited onto the γ-phase free substrate on the other hand does not present such preferred <110> texture. The functionally graded surfaces present different microstructure characteristics, which may influence the nucleation and growth of the nitride and carbonitride layer, i.e. the γ-phase free gradient present higher cobalt content, reduced WC surfaces and lower nitrogen content compared to the γ-phase rich surface and the non-graded microstructures. However, in this work the influence of texture was not considered in the calculation of the residual thermal stresses.

The chemical N/C gradient of the Ti(C,N) layers was characterized by EPMA. This gradient also induces a gray-to-yellow color gradient in the Ti(C,N) coating layers, as observed in the optical microscope images of Fig. 1. Fig. 3 shows the atomic concentration ratio N/C (EPMA data) as a function of the Ti(C,N) coating thickness. This data was then used to estimate the Ti(C,N) lattice parameter variation using Eq. 4:

$$a_{Ti(C,N)}[\text{nm}] = \frac{0.00857}{1+\dfrac{N}{C}} + 0.42417 \qquad (4)$$

where C and N denotes atomic concentrations for carbon and nitrogen ranging from 0 to 1. The Ti(C,N) lattice increases exponentially as a function of the coating depth, as shown in Fig. 3. The lattice parameter gradient influences the value of the *d(hkl)*-spacing measured by XRD and therefore must be taken into account when applying the standard $\sin^2\psi$ method [10] to estimate stresses. In this regard, the scattering vector method [11] is used to determine the in-depth strain-free d0(hkl) spacings and thus allow for discarding the effect of the chemical gradient on the stress measurements.

3.2. EDXRD analysis

As an example of the data acquired during the experiment, the EDXRD spectra obtained during $\sin^2\psi$ measurements on the as-coated Ti(C,N)/substrate systems (Table 1) at $\psi = 72°$ before the thermal cycling (25°C) are shown in Fig. 4. The 111, 200, and 220 reflections of the Ti(C,N) phase were used to estimate the coating stress. It is worth to note that although the systems have different substrates, the reflections of the WC bulk and Ti(C,N) coating showed similar signal-to-noise ratio during the measurements.

The distributions of the d_0^{hkl}-spacings of Ti(C,N) as a function of the penetration depth were acquired by the scattering vector method on the as-coated and blasted systems at room temperature and at 800 °C. No significant differences were observed in the scattering vector data within different sample conditions, indicating that the chemical gradient was not strongly affected by blasting or the graded substrate layer. As an example of the data reduction Fig. 5A shows the d(200)-spacing of the Ti(C,N) coating phase measured by the scattering vector method in the as-coated Ti(C,N)/substrate A system before the thermal cycle. The strongly nonlinear dependence shown is due to the chemical gradient in the Ti(C,N) coating. The scattering vector data allow for transforming each d^{hkl}-$\sin^2\psi$ distribution obtained by the standard $\sin^2\psi$ measurement into an ε^{hkl}-$\sin^2\psi$ distribution corrected regarding the in-depth d_0-variation. Moreover, Fig. 5B shows the lattice parameter of the Ti(C,N) phase estimated by the scattering vector method using the three different reflections as a function of the penetration depth (τ) for the same Ti(C,N)/substrate A system and experimental conditions. It is worth to note that the nonlinearity of these curves evidences the chemical C/N gradient in the coating, which stabilizes for $\tau > 18$ μm.

As an example the corrected ε^{hkl}-$\sin^2\psi$ distributions for the Ti(C,N) reflections obtained by taking into account the chemical d_0^{hkl}-gradient together with the weighed-averaged distribution considering the multiplicity factors of each reflection are shown in Fig. 6.

The variations between the different regression results for each hkl are in the same order of magnitude as the linear regression errors, therefore no significant differences in the stress values for different hkl are reported. X-ray elastic constants (-s1 and s2/2) for specific hkl were considered in the stress estimations. These were calculated using the Eshelby-Kroener model and the single-crystal compliances of TiN.

3.3. FEM Results

When a linear-elastic stress model was applied (Model I), the compressive in-plane stresses

from only thermal expansion mismatches in the coatings were calculated to be about 100 MPa at the final CVD deposition temperature of 1050 °C. After cooling, the room-temperature stresses were found to be well above the estimated tensile yield limits. Directly after the coating process the coating was found to be subjected to thermal tensile stresses exceeding 1000 MPa at room temperature (25 °C). When re-heating to 800°C, the calculated stresses were still found tensile at about 200 MPa.

Using linear-elastic stress, reasonable agreement between measurements and modeling of thermal strains (in plane/out-of-plane) at both room temperature and 800 °C could only be reproduced if uniform in-plane compressive stresses of around 650 MPa were introduced at deposition temperatures (Model II).

A simple deformation mechanism introducing bi-linear plasticity was also used to calculate strain relationships in agreement with measurements (Model III). Using this model tensile yield was reached gradually through the coating layers at around 600 °C during cooling after the coating process.

Calculated average stresses through coatings during thermal cycling are illustrated for the Ti(C,N)/substrate C system in Fig. 7. In the figure, the results from different thermal load steps are spaced along the horizontal axis to reflect constant temperature change rates. This gives good overviews for the stress vs. temperature relationships for Model I and Model II while also illustrating how thermal load history affects the stresses calculated from Model III. It could be noted that there are no rate dependencies in any of the models used, which means the load step spacings in Fig. 7 have no relationship to time. The dotted plot, representing Model II, is based on the calculations that were used to evaluate Model I, but for Model II the stresses were offset for the best possible match with the experimental results. In the calculations using the model with bi-linear plasticity the tensile and compressive yield stresses were both set to 350 MPa based on comparisons between calculated and measured

13

elastic strains, and tangent moduli in the yield regions were set to 1 GPa to represent a near-ideal plastic material. All values in Fig. 7 represent stresses which have been averaged and thickness-weighted through all coating layers along the rotational symmetry axis.

4. Discussion

As presented in the summary of stresses during the single thermal cycling (Fig. 8) tensile stresses develop within the Ti(C,N) coatings in the as-coated condition, indicating that thermal strains represent the major source of residual stresses in the present case. A rough estimation of the thermal stress in the coating is given by:

$$\sigma = (Y_{M\,layer} / 1 - \upsilon_{layer}) (\alpha_{HM} - \alpha_{layer}) (RT - T_{max}) \qquad (5)$$

where $Y_{M\,layer}$, υ_{layer} and α_{layer} are the Young modulus, the Poisson ratio and the TEC of Ti(C$_{0.2}$N$_{0.8}$) taken from Ref. [17]; Y_{Mlayer}= 410 GPa, υ_{layer}= 0.224, α_{layer} = 9.2 10^{-6}/K; RT is room temperature and T_{max} is the average deposition temperature of the CVD process, T_{max}= 950°C. The TEC values for the graded substrates are given in Table 1.

The estimated thermal stresses are $\sigma_A \approx$ 1990 MPa (280 ± 40 MPa measured), $\sigma_B \approx$ 1890 MPa (420 ± 40 MPa measured) and $\sigma_C \approx$ 1400 MPa (240 ± 30 MPa measured). As observed, the theoretical and measured values differ considerably in magnitude. One possible reason is the presence of defects such as cracks in the CVD layers, which are unavoidable to form during the cooling step of the CVD process due to the strong differences between TECs of the thin films and the hard metal substrates, and to the ceramic-like behavior of the carbonitride coating, with reduced plastic deformation. Cracks may release stresses within the layer considerably. Interestingly higher stress values were measured for the Ti(C,N) deposited on sample B despite of the same deposition parameters. Sample B presents a tough gradient surface layer (γ-phase free layer) with a lower hardness compared to samples A (no gradient)

and sample C (γ-phase rich layer), which may increase the stress level of the Ti(C,N) layer since the softer substrate may allow for a higher deformation of the carbonitride layer. Another effect to be considered is the different texture of the Ti(C,N) deposited on sample B compared to the texture of coating in sample A and C. As shown in the EBSD analysis (Fig. 2) the Ti(C,N) coating on this substrate did not show the <110> texture observed in the A and C samples, which may indicate that the presence of a preferential fiber texture may influence the residual stress of the coating after deposition.

Induced compressive stresses on multilayer coatings, in particular for Al_2O_3-based coatings [5,25,26], is extensively used in the cutting tool industry to improve the performance during machining. Compressive stresses in the Ti(C,N) coating after blasting suggests that the mechanical impact energy of the Al_2O_3 particles onto the coating surface is able to plastically deform the Ti(C,N) film. This effect has been also reported for TiN coatings after blasting [25]. The analysis of the diffractograms in blasted TiN CVD layers showed that anisotropic nano-structural changes on the surface of the thin film takes place, leading to compressive stresses in the outer-surface region of few µm.

The effect of blasting on the coating is directly correlated with the toughness of the functionally graded substrates. Indeed the tough γ-phase free substrate (B) allowed compressive stresses of around $\sigma \approx$ -1000 MPa on the coating, whereas the hardmetal (A) and γ-phase rich (C) substrates allowed around half of this value. Again higher compressive stresses were achieved on sample B despite of same blasting treatment, which could indicate the influence of the tougher gradient transition to the coating (γ-phase free layer) and/or a different behavior of the blasting treatment due to the weak texture of the carbonitride layer on sample B.

On heating up to 800°C, both the as-deposited and blasted coatings evolve compressive stresses which are released by cooling down to RT again. The reduction of compressive stresses from RT to 800°C in the top-blasted samples may follow similar relaxation phenomena as described in Ref. [25]. Bartosik et al. plotted the temperature dependence of volume averaged residual stresses in blasted TiN coatings, where they recognized four segments for the stress evolution from RT to 1100°C. Thus, the relaxation of macroscopic residual stresses may be accompanied by nanostructural changes like crystallite growth and remove of point defects by diffusion and migration/annihilation of dislocations.

In Fig. 8 it can be observed that, for the blasted samples, the compressive stresses turn into tensile stresses after the heating cycle, reaching values of around 150 to 500 MPa, depending on the substrate/coating system. This thermo-elastic change of residual stress direction may be controlled by the relative TEC of the coating and substrate systems since they follow the expected tendencies regarding TEC differences between the tougher functionally graded substrates (A and B) and the harder one (C).

However, for as-deposited coating without blasting, this is a remarkable effect which may indicate that strong microstructural changes take place during the CVD cooling step and the heating step in the Ti(C,N) coating. This may onset the stress free temperature of the coating to values considerable below the deposition conditions, so that high compressive residual stresses can develop in the thin film when heated at a temperature of 800°C, which is below the final deposition temperature of the film (1050°C).

Regarding the FEM modeling it must be pointed out that the material models in the present work are based on bulk materials and not on thin films. Subdivision of a coating film into layers of isotropic compositions does not reproduce the material property gradients in detail, and the present treatment of each layer as deposited in a stress-free state has no basis in

16

experimental data.

However, even considering very large combined uncertainties in modeling and in measurements, it is apparent due to excessive tensile stresses that it is not possible to describe residual stresses in the coating after deposition and cooling to room temperature with a linear-elastic behavior. Stresses from thermal contraction would fracture the coating, and to predict a stress-strain relationship for even more increased deformation would require more detailed models.

For a non-fractured material, the calculations can be reasonably fitted to the measurements if initial stresses caused by the coating process are introduced or if plasticity is considered. A range of stress states can develop in many thin films during deposition, and compressive stresses have previously been studied by e.g. Chason et al. [27]. Considering initial in-plane compressive stresses, curves from measurements during thermal cycling would be symmetric both around temperature maxima and minima. For comparison, in a scenario with near-ideal plastic material deformation, elastic stresses during cycling would reach a temperature limit below which they would become measured as nearly constant if cooling continued. But upon heating the stresses would quickly decrease again, even if temperatures were still below the limit. A dislocation creep mechanism during the controlled thermal expansion and contraction of the coating could result in such plastic deformation. Stress measurements at additional temperatures could rule out or provide further information for the suggested models by comparing the thermal cycling behaviors.

5. Conclusions

- The as deposited Ti(C,N) thin films present a cycling residual thermal stress behavior (tensile-compressive-tensile) connected to the temperature cycle. The stress level varies if the coatings are as-coated or top-blasted. If top-blasting is applied on the thin

film layer after the coating process compressive stresses are generated. These compressive stresses are released after the high temperature thermal cycle.

• The measured stresses are below the theoretical stresses, which may originate due to TEC differences. This indicates that stresses are released due to known crack formation during the cooling step of the CVD process.

• Other type of defects may originate in the coating during CVD cooling and posterior heating, which may set up a stress-free condition in the coating layer far below the deposition temperature of the layer. This may explain the high compressive stresses measured when the coatings were heated below their deposition temperature.

• The FEM results of the in-plane stresses in the rotation-symmetric coating during thermal load cycling are in best agreement with the measured stress values when a plasticity model is introduced to the FEM model.

• It is shown that the introduction of functionally graded cemented carbide surfaces has an effect on the stress level when the coatings are blasted. The graded surfaces do not provide considerably advantage concerning the reduction or matching of stresses in a thermal cycling condition in the as-coated condition. However in the blasted condition, the stress level in the coating film is lower if a Ti(C,N)-enriched surface is present in the cemented carbide.

• Despite of the functionalization of the surface of the cemented carbides, the alternating stress behavior cannot be avoided indicating that the overall composition

of the cemented carbide strongly affects the stress behavior of the coating/substrate systems. This is in accordance with experience about microstructural features in cemented carbides which are detrimental for avoiding/reducing the formation of comb cracks: the increment of the volume fraction of cobalt (as in the γ-free graded layers) and the increment of volume fraction of cubic carbide phase (as in the γ-rich graded layers).

Acknowledgements

References

[1] Prakash L. Fundamentals and General Applications of Hardmetals, in: Vinod K. Sarin (Ed.), Comprehensive Hard Materials, Elsevier, 2014: pp. 29-90.

[2] Mitterer C. PVD and CVD Hard Coatings, in: Vinod K. Sarin (Ed.), Comprehensive Hard Materials, Elsevier, 2014: pp. 449-467.

[3] Bleeck O, Munz D, Schaller W, Yang YY. Effect of a graded interlayer on the stress intensity factor of cracks in a joint under thermal loading. Eng Fracture Mech 1998;60(5-6):615-23.

[4] García J, Pitonak R. The role of cemented carbide functionally graded outer-layers on the wear performance of coated cutting tools. Int J Refrac Met Hard Mater 2013;36:52-9.

[5] Barbatti C, García J, Pinto H, Kostka A, Di Prinzio A, Staia M, Pitonak R, Pyzalla A. Influence of micro-blasting on the microstructure and residual stresses of CVD κ-Al2O3 coatings. Surf Coat Techn 2009;203:3708–17.

[6] Riedl A, Schalk N, Czettl C, Sartory B, Mitterer C. Tribological properties of Al_2O_3 hard coatings modified by mechanical blasting and polishing post-treatment. Wear 2012; 289:9-16.

[7] Pandey PC, Bhatia SM, Shan HS. Thermo-mechanical failure of cemented carbide tools in intermittent cutting. CIRP Ann. 1979;28:13–7.

[8] Teppernegg T, Klünsner T, Angerer P, Tritremmel C, Czettl C, Keckes J, Ebner R, Pippan R. Evolution of residual stress and damage in coated hard metal milling inserts over the complete tool life. Int J Refrac Metals Hard Mat 2014;47:80-5.

[9] García J, Pitonak R, Weissenbacher R, Köpf A. Production and characterization of wear resistant Ti(C,N) coatings manufactured by modified chemical vapor deposition process. Surf Coat Techn 2010;205:2322–27.

[10] Noyan IC, Huang TC, York BR. Residual stress/strain analysis in thin films by X-ray diffraction. Crit Rev Sol State Mat Sci 1995;20:125–77.

[11] Genzel C. Formalism for the evaluation of strongly non-linear surface stress fields by X-ray diffraction performed in the scattering vector mode. Phys Status Sol 1994;146:629–37.

[12] Noyan IC, Cohen JB. Residual stress: measurement by diffraction and interpretation, Springer Verlag, 1987.

[13] Genzel C, Denks IA, Gibmeier J, Klaus M, Wagener G. The materials science synchrotron beamline EDDI for energy-dispersive diffraction analysis, Nuclear Instruments and Methods, in Physics Research Section a: Accelerators, Spectrometers, Detectors and Associated Equipment 2007;578, pp. 23–33.

[14] Ramos-Moore E, Espinoza C, Coelho RS, Pinto H, Brito P, Soldera F, Mücklich F, García J. Investigations on thermal stresses of a graded Ti(C,N) coating deposited on WC-Co

hardmetal. Adv Mat Res 2014;996:848–54.

[15] Steneteg P, Hellman O, Vekilova O, Shulumba N, Tasnádi F, Abrikosov IA. Temperature dependence of TiN elastic constants from ab initio molecular dynamics simulations. Phys Rev B 2013;87: 094114.

[16] Mathe BA, Comins JD, Every AG, Lengauer W. Thermal dependence of elastic properties of polycrystalline $TiC_{0.97}$ and $TiC_{0.40}N_{0.60}$ alloys studied by surface Brillouin scattering. Int J Refract Met Hard Mater 2014;45:212-17.

[17] Kral C, Lengauer W, Rafaja D, Ettmayer P. Critical review on the elastic properties of transition metal carbides, nitrides and carbonitrides, J Alloy Comp 1998;265 : 215-33.

[18] Karlsson L, Hultman L, Johansson MP, Sundgren JE, Ljungcrantz H. Growth, microstructure, and mechanical properties of arc evaporated TiC_xN_{1-x} (0 = x = 1) films. Surf Coat Technol 2000;126:1-14.

[19] Aigner K, Lengauer W, Rafaja D, Ettmayer P. Lattice Parameters and thermal expansion of $Ti(C_xN1-x)$, $Zr(C_xN_{1-x})$, $Hf(C_xN_{1-x})$, and TiN_{1-x} from 298 to 1473 K as investigated by high-temperature X-ray diffraction. J Alloys Comp 1994;2:121-26.

[20] Shackelford JF, Alexander W. CRC Materials Science and Engineering Handbook, Third Edition, CRC Press LLC, Boca Raton, 2000.

[21] García J, Lindwall G, Prat O, Frisk K. Kinetics of formation of graded layers on cemented carbides: Experimental investigations and DICTRA simulations. Int J Refrac Met Hard Mater 2011;29:256–59.

[22] Barbatti C, García J, Sket F, Kostka A, Pyzalla AR. Influence of nitridation on surface microstructure and properties of graded cemented carbides with Co and Ni binders. Surf Coat Techn 2008;202:5962–75.

[23] García J, Pitonak R, Agudo L, Kostka A. Synthesis of titanium carbonitride coating layers with star-shaped crystallite morphology. Mat Letters 2011;68:71–4.

[24] García J, Pitonak R, Weissenbacher R, Köpf A, Soldera F, Suarez S, Miguel F, Pinto H, Kostka A, Mücklich F. Design and Characterization of Novel Wear Resistant Multilayer CVD Coatings with Improved Adhesion Between Al_2O_3 and Ti(C,N). Adv Eng Mater 2010;12:929–34.

[25] Bartosik M, Pitonak R, Keckes J. In situ high temperature X-ray diffraction reveals residual stress depth-profiles in blasted TiN hard coatings. Adv Eng Mat 2011;13(8)705-11.

[26] Klaus M, Genzel Ch, Holzschuh H. Residual stress depth profiling in complex hard coating systems by X-ray diffraction. Thin Solid Films 2008;517:1172-76.

[27] Chason E, Shin JW, Hearne SJ, Freund LB. Kinetic model for dependence of thin film stress growth rate, temperature, and microstructure. J Appl Phys 2012;111: 083520.

FIGURES
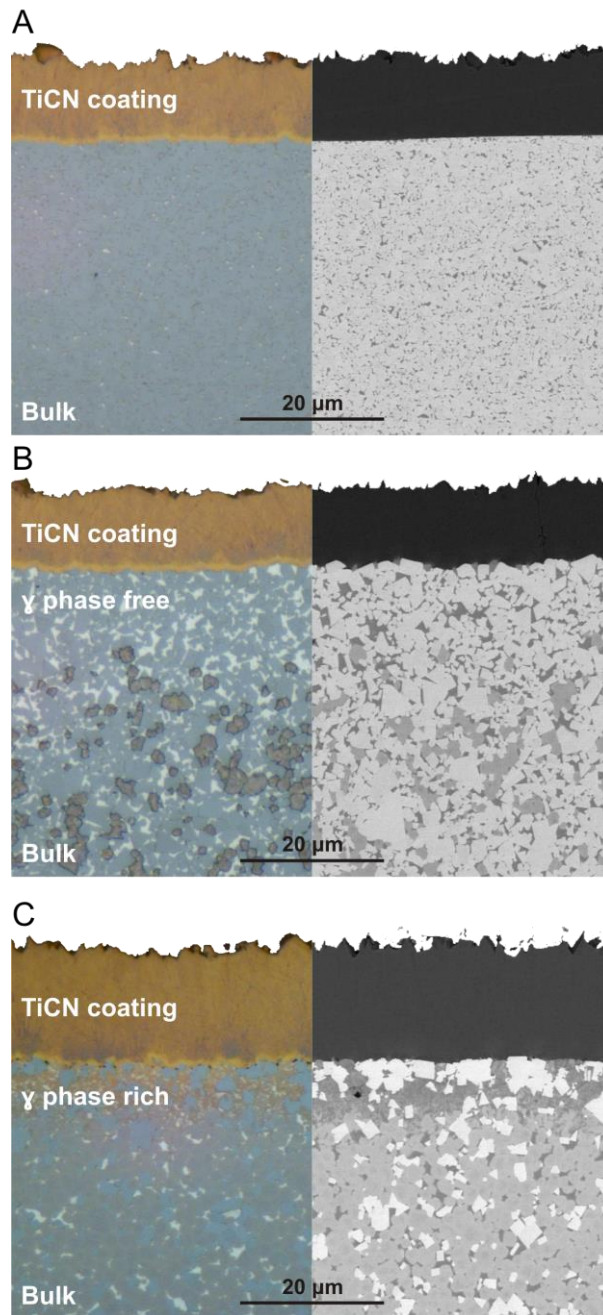
Fig. 1. Optical (left) and SEM (right) images of the tools systems. As resumed in Table 1, substrate 1 is WC-Co cemented carbide (top), substrate 2 is cemented carbide with tough-graded layers (middle) and substrate 3 is cemented carbide with wear-resistant layers (bottom).
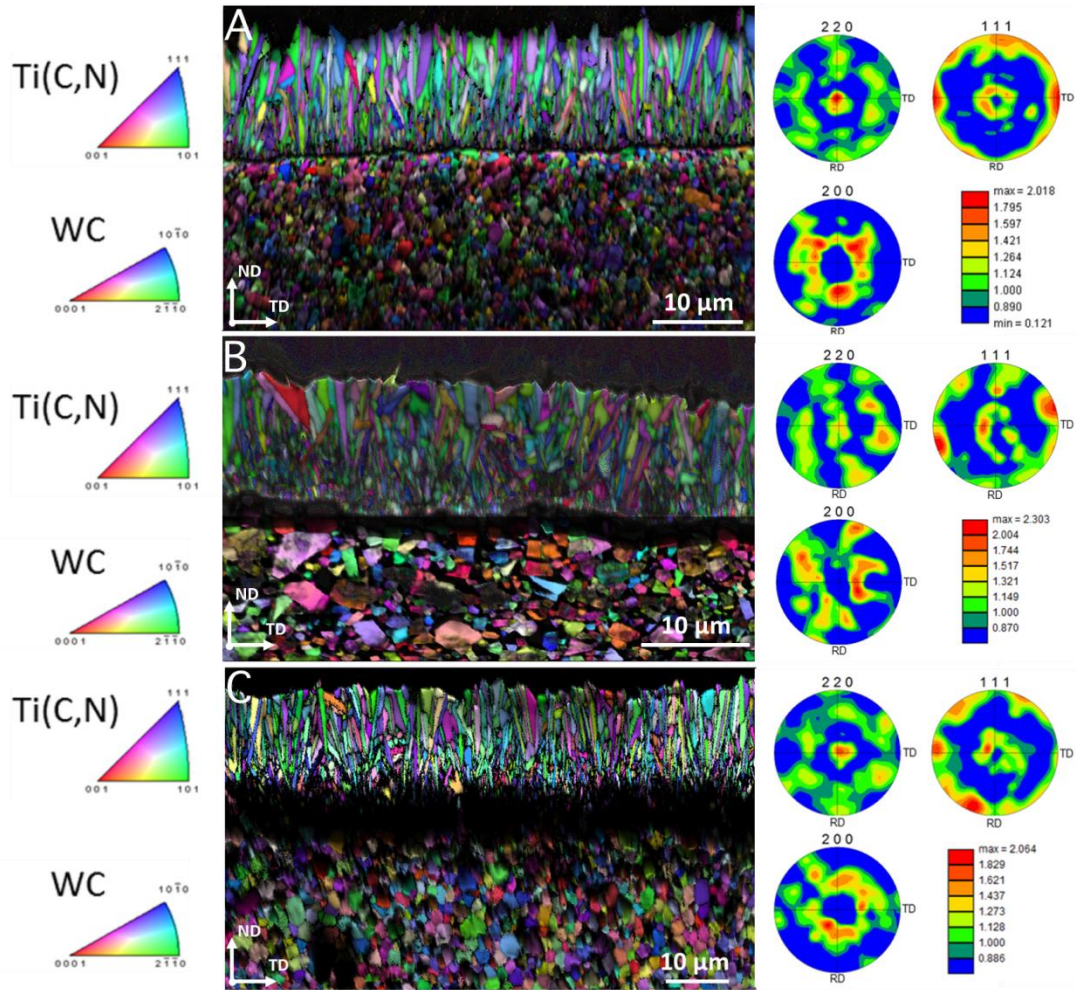
Fig. 2. EBSD inverse pole figure maps of the as-coated tool systems show in Fig. 1. A) Ti(C,N)/substrate A system, B) Ti(C,N)/substrate B system and C) Ti(C,N)/substrate C system (see Table1).
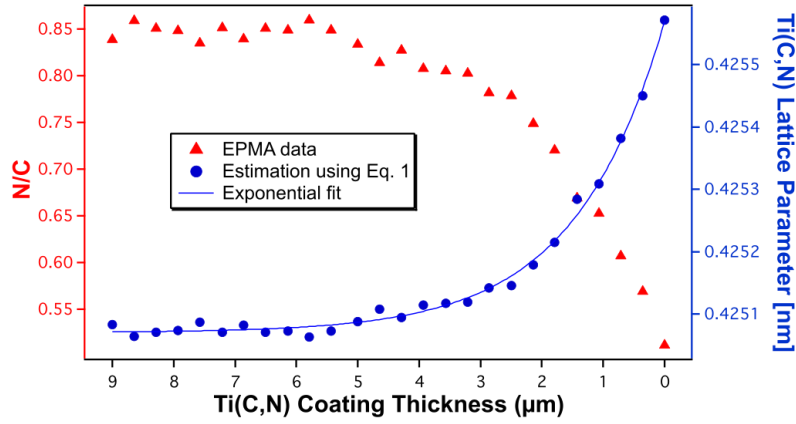
Fig. 3. EPMA data of the as-fabricated sample showing the elemental ratio N/C as a function of the Ti(C,N) coating thickness. The Ti(C,N) lattice parameter estimated using Eq. 1. decreases exponentially as the thickness increases.
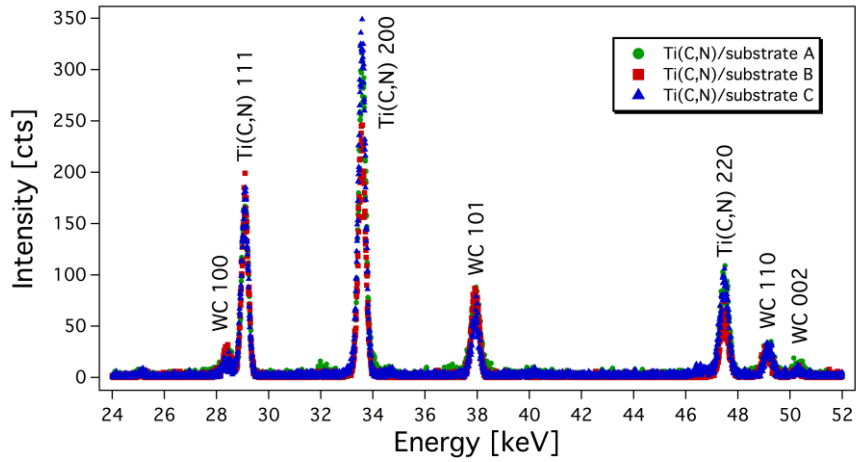
Fig. 4. ED spectra of the as-coated Ti(C,N)/substrate systems (Table 1) measured before the thermal cycling (25 °C) at $\psi = 72°$. Although the substrates differ, the reflections of the WC bulk and Ti(C,N) coating show similar signal-to-noise ratio. Reflections 111, 200 and 220 of Ti(C,N) were used to estimate the coating stress.
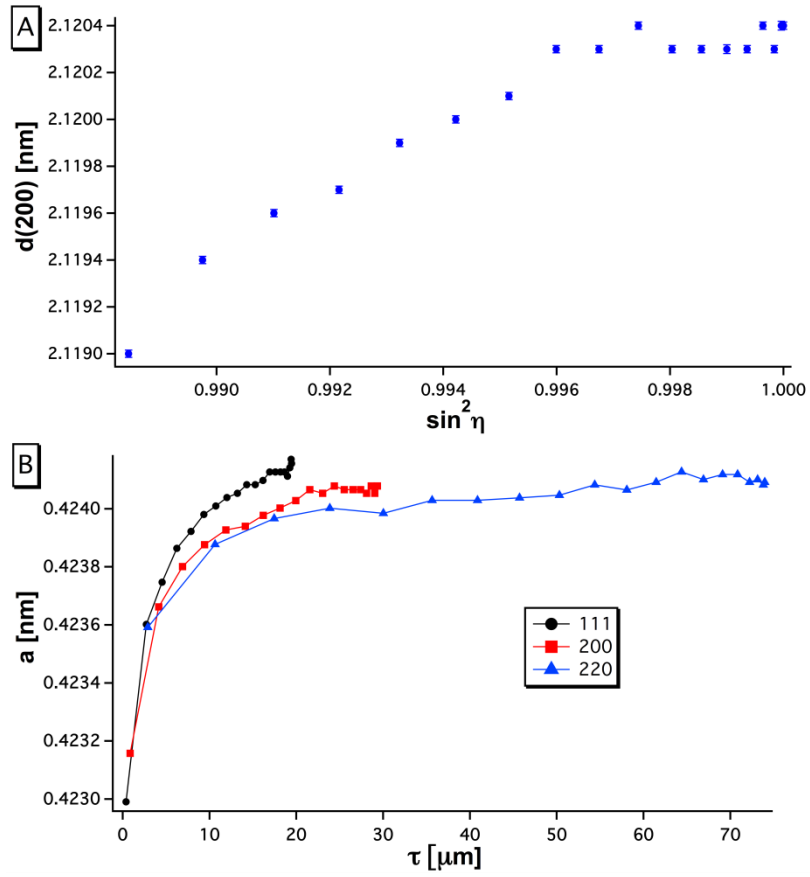
Fig. 5. A) 200 Lattice spacing variation for Ti(C,N) as determined by the scattering vector method in the as-coated Ti(C,N)/substrate A system. B) Lattice parameter of Ti(C,N) (a) as a function of the penetration depth (τ), as determined by the scattering vector method in the same system.
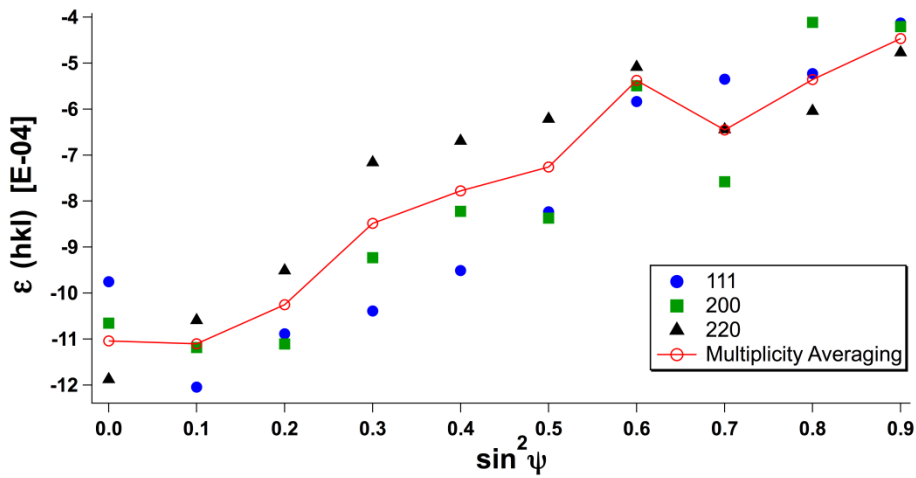

Fig. 6. Corrected ε^{hkl}-$\sin^2\psi$ distributions for the Ti(C,N) reflections obtained by taking into account the chemical $d_0$hkl-gradient together with the weighed-averaged distribution considering the multiplicity factors of each reflection.
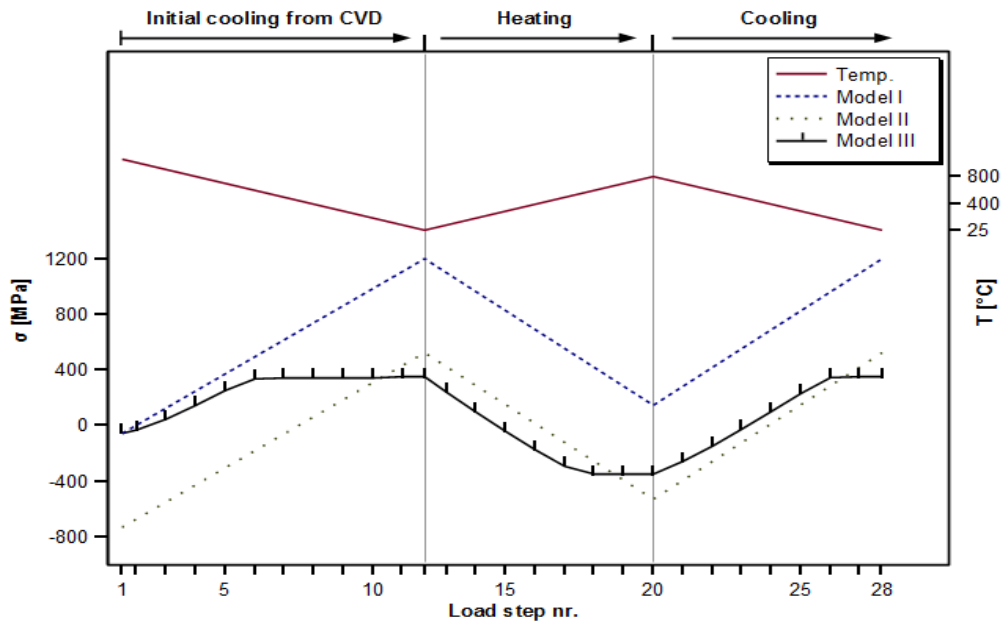
Fig. 7. Modeled in-plane stresses in the rotation-symmetric coating during thermal load cycling for sample C. Example show the cases of a linear-elastic stress (model I), a linear-elastic model with in-plane compressive stresses (model II), and a model with bi-linear plasticity (model III).
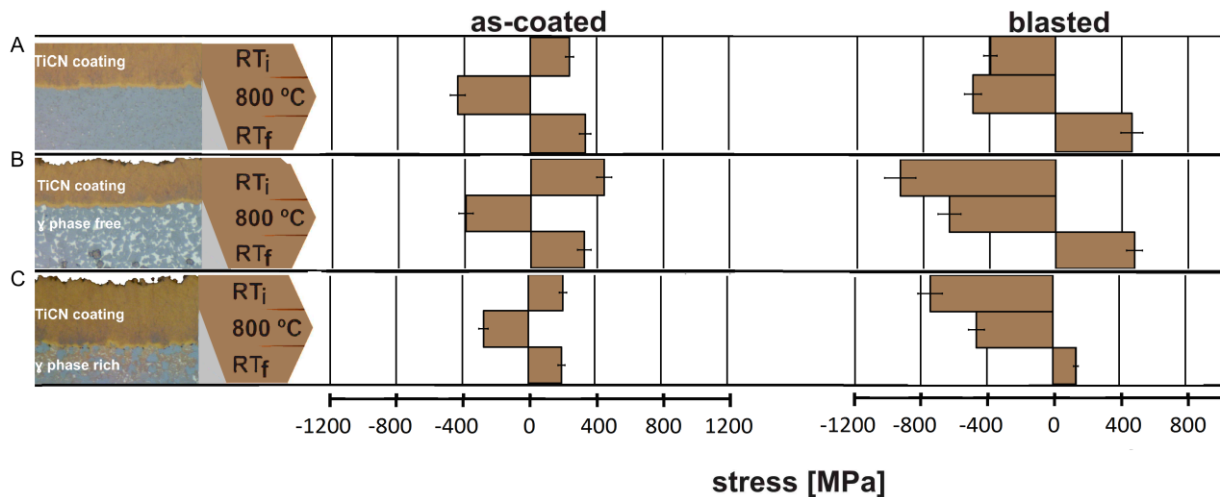

Fig. 8. Summary of stresses in the Ti(C,N) coating layer at the three stages of the thermal cycle: room temperature initial (RT$_i$), high temperature (800 °C) and room temperature final (RT$_f$).